

Chemistry A European Journal

 **Chemistry
Europe**
European Chemical
Societies Publishing

Accepted Article

Title: Yet Another Case of Lithium Metal Atoms and Germanium Atoms Sharing Chemistry in the Solid State: Synthesis and Structural Characterization of Ba₂LiGe₃

Authors: Kowsik Ghosh and Svilen Bobev

This manuscript has been accepted after peer review and appears as an Accepted Article online prior to editing, proofing, and formal publication of the final Version of Record (VoR). The VoR will be published online in Early View as soon as possible and may be different to this Accepted Article as a result of editing. Readers should obtain the VoR from the journal website shown below when it is published to ensure accuracy of information. The authors are responsible for the content of this Accepted Article.

To be cited as: *Chem. Eur. J.* **2023**, e202302385

Link to VoR: <https://doi.org/10.1002/chem.202302385>

Yet Another Case of Lithium Metal Atoms and Germanium Atoms Sharing Chemistry in the Solid State: Synthesis and Structural Characterization of Ba_2LiGe_3

Kowsik Ghosh,^[a] and Svilen Bobev*^[a]

[a] Dr. K. Ghosh, Prof. S. Bobev
Department of Chemistry and Biochemistry
University of Delaware
Newark, Delaware 19716, United States
E-mail: bobev@udel.edu

Supporting information for this article is given via a link at the end of the document.

Abstract: Several Ba–Li–Ge ternary phases are known and structurally characterized, including the title compound Ba_2LiGe_3 . Its structure is reported to contain $[\text{Ge}_6]^{10-}$ anions that exhibit delocalized bonding with a Hückel-like aromatic character. The Ge atoms are in the same plane with the Li atoms, and if both types of atoms are considered as covalently bonded, $[\text{LiGe}_3]^{4-}$ honeycomb-like layers will result. The latter are separated by slabs of Ba^{2+} cations. However, based on the systematic work detailed herein, it is necessary to re-evaluate the phase as $\text{Ba}_2\text{Li}_{1-x}\text{Ge}_{3+x}$ ($x < 0.05$). Although small, the homogeneity range is clearly demonstrated in the gradual change of the unit cell for four independent samples. Subsequent characterization by single-crystal X-ray diffraction methods shows that the $\text{Ba}_2\text{Li}_{1-x}\text{Ge}_{3+x}$ structure, responds to the varied number of valence electrons and the changes are most pronounced for the refined lengths of the Li–Ge and Ge–Ge bonds. Indirectly, the changes in the Ge–Li/Ge distances within layers affect the stacking too, and these changes can be correlated to the variation of the *c*-cell parameter. Chemical bonding analysis based on TB-LMTO-ASA level calculations affirms the notion for covalent character of the Ge–Ge bonds; the Ba–Ge and Li–Ge interactions also show some degree of covalency.

Introduction

Reacting, in the solid state, alkali metals and/or alkaline-earth metals with the metalloids (early p-block elements) generates a large number of compounds with unusual structures [1–14]. In particular, one should notice that the structural diversity is greatly amplified if the realization of compounds containing more than one type of alkali metals and/or alkaline-earth metals are considered [7–14]. The different nature/ratios of elements in the chemical make-up of the compound leads to varied bonding arrangements, where the atoms of the metalloid use the electrons donated by the alkali metals or alkaline-earth metals and form 2D- or 3D-networks, chains and chain-like fragments, small clusters, dumbbells, etc. This is the essence of the Zintl concept [15,16], which is typically applied to rationalize such structures, considering the electronegativity differences and the octet rule.

On this extension, germanium, when reacted with alkali or alkaline-earth metals, forms binary germanides that exhibit all of the above. Specifically, one can find a 3D-network in the structure of LiGe [17], puckered 2D-sheets in the structure of CaGe_2 [18], 1D-chains in CaGe , SrGe and BaGe [19–21], small isolated cluster anions in BaGe_2 and Cs_4Ge_9 in [22,23], etc. Germanium in a combination with the lightest alkali metal, lithium and the heaviest (non-radioactive) alkaline-earth metal, barium, affords the following Ba–Li–Ge ternary phases: BaLi_2Ge (isolated Ge^{4-} anion) [24], Ba_2LiGe_3 (isolated $[\text{Ge}_6]^{10-}$ anion) [25], BaLiGe_2 (cis-trans $[\text{Ge}_2]^{3-}$ chain) [26], and $\text{Ba}_8\text{Li}_5\text{Ge}_{41}$ (open 3D-framework) [27]. The structures of Ba_2LiGe_3 and BaLiGe_2 have no precedent among the respective binary phases.

For the past 6–7 years, we have been studying the lithiation behavior of Ge-based clathrates [27–29]. Over the course of our work, we often observed the presence of some of the above-mentioned ternaries as reaction byproducts. One particular experimental observation piqued our attention, namely, the small mismatch between the observed and simulated powder X-ray diffraction patterns for Ba_2LiGe_3 [25]. Initially, we had no reasonable hypothesis as to why this might be the case, but potential breakthrough came to light when we synthesized and characterized the type-I clathrate $\text{Ba}_8\text{Li}_5\text{Ge}_{41}$ (or rather $\text{Ba}_8\text{Li}_x\text{Ge}_{46-x}$ ($x < 5.33$), where Li/Ge disorder was observed [27]. Our results, based on single-crystal X-ray diffraction work, showed the existence of Li occupying a crystallographic site nominally taken by Ge. This shared chemistry between lithium and germanium atoms in the solid state contributes to subtle changes in the unit cell volume and subsequent small peak-shifts when experimental and simulated powder X-ray diffraction patterns are compared.

Given the above, we set out to re-assess the crystal structure of Ba_2LiGe_3 that was reported by the von Schnering team more than 25 years ago [25]. Here, we report on the plausible Li/Ge disorder in this compound that has remained undetected for decades. In order to have sufficient data to model the stipulated disorder, and understand its effect, we synthesized four different samples with slightly Li-deficient $\text{Ba}_2\text{Li}_{1-x}\text{Ge}_{3+x}$ ($x < 0.1$) and Li-rich $\text{Ba}_2\text{Li}_{1+x}\text{Ge}_{3-x}$ ($x < 0.1$) nominal compositions. All obtained crystals were characterized by single-crystal and powder X-ray diffraction. The results do confirm a small homogeneity range for

$\text{Ba}_2\text{Li}_{1-x}\text{Ge}_{3+x}$ ($x < 0.05$), which is clearly demonstrated in the variations of the unit cell volumes and the concomitant changes for the refined lengths of the Li–Ge and Ge–Ge bonds. Electronic structure calculations were also carried out to further study the nature of the chemical bonding.

Materials and Methods

Synthesis

Samples of $\text{Ba}_2\text{Li}_{1-x}\text{Ge}_{3+x}$ were synthesized by fusing the elements together in an induction furnace. From each sample, many single-crystals were analyzed; for the best four independent single-crystals, named A, B, C, and D, intensity data were collected and analyzed (*vide infra*). All work was carried out under protective atmosphere or under vacuum since both the starting materials and the products are unstable in air.

The elements Ba, Li, and Ge were purchased from Sigma-Aldrich and Alfa Aesar with a purity $\geq 99.9\%$ wt. The surface of Li rod was cleaned with a scalpel blade immediately before use it. Argon gas-filled glovebox with $\text{O}_2/\text{H}_2\text{O}$ levels below 1 ppm was utilized for this purpose. A, B samples were the slightly Li-deficient ones, and C, D samples had Ba : Li : Ge ratio of 2 : 1.1 : 2.9. The elemental mixtures were then put into Nb-tubes, which were subsequently welded shut under argon atmosphere. The closed niobium tubes were then put into evacuated fused silica tubes and heat-treated using an induction furnace. All the reactions were carried out under identical conditions. The reactions were performed at temperature of 1223 K, measured

by a pyrometer, for 5 min 30 sec, and then cooled to 973 K (30 sec) before the furnace was switched off and the specimens cooled to room temperature. Then, the welded tubes were brought back in the glove box and cut open to recover the products.

Powder X-ray Diffraction (PXRD)

Powder X-ray diffraction (PXRD) measurements were carried out at room temperature on a Rigaku Miniflex diffractometer (filtered Cu $K\alpha$ radiation, $\lambda = 1.5418 \text{ \AA}$), operated inside a nitrogen-filled glovebox. Small portions of the obtained single crystals were ground into powder using agate mortars and pestles. The data were collected between 5 and 75° in 2θ with a step size of 0.05° and 2 s per step counting time. The PXRD measurements before and after exposure to air over a period of only 10 min show that the phase decomposes.

Single-crystal X-ray Diffraction (SCXRD)

Suitable single-crystals were selected and were cut under dry Paratone-N oil to appropriate dimensions ($\leq 0.10 \text{ mm}$). This was done using the microscope in the glovebox. After that, crystals were taken out, brought to the diffractometer, quickly scooped by MiTeGen plastic loops and transferred to the goniometer. Experiments were conducted under the protective stream of cold nitrogen and temperature was maintained at 200(2) K. Many crystals were tried before the best ones were chosen.

Table 1. Selected crystallographic data for $\text{Ba}_2\text{Li}_{1-x}\text{Ge}_{3+x}$. The synthesized samples are labeled as A, B, C, and D, with A and B having slightly Li-deficient nominal compositions, while the C and D samples have slightly Li-rich nominal compositions. For all four crystals, $T = 200(2) \text{ K}$; Mo $K\alpha$, $\lambda = 0.71073 \text{ \AA}$; space group $Fddd$, $Z = 16$. For comparison, the reported unit cell parameters for Ba_2LiGe_3 are: $a = 8.901(1) \text{ \AA}$, $b = 15.469(2) \text{ \AA}$, and $c = 19.4300(20) \text{ \AA}$ (room temperature).

Sample	A	B	C	D
Refined chemical formula	$\text{Ba}_2\text{Li}_{0.95}\text{Ge}_{3.05(1)}$	$\text{Ba}_2\text{Li}_{0.96}\text{Ge}_{3.04(1)}$	$\text{Ba}_2\text{Li}_{0.96}\text{Ge}_{3.04(1)}$	Ba_2LiGe_3
$a / \text{ \AA}$	8.915(3)	8.895(2)	8.8707(18)	8.8873(19)
$b / \text{ \AA}$	15.508(5)	15.467(4)	15.413(3)	15.445(3)
$c / \text{ \AA}$	19.109(6)	19.190(5)	19.360(4)	19.356(4)
$V / \text{ \AA}^3$	2641.9(14)	2640.3(12)	2646.9(9)	2656.8(9)
$\rho_{\text{calc.}} / \text{ g cm}^{-3}$	5.06	5.05	5.04	5.00
$\mu_{(\text{Mo-K}\alpha)} / \text{ cm}^{-1}$	253.2	252.8	252.2	249.6
$R_1 (I > 2\sigma(I))^{[a]}$	0.0354	0.0324	0.0332	0.0287
$wR_2 (I > 2\sigma(I))^{[a]}$	0.0793	0.0665	0.0641	0.0562
R_1 (all data) ^[a]	0.0791	0.0758	0.0736	0.0696
wR_2 (all data) ^[a]	0.0943	0.0888	0.0769	0.0735
$\Delta\rho_{\text{max,min}} / \text{ e}^{-} \cdot \text{ \AA}^{-3}$	1.22, -1.47	1.32, -1.82	1.12, -1.49	1.47, -1.08

[a] $R_1 = \sum |F_o| - |F_c| / \sum |F_o|$; $wR_2 = [\sum [w(F_o^2 - F_c^2)^2] / \sum [w(F_o^2)^2]]^{1/2}$, where $w = 1 / [\sigma^2(F_o^2) + (xP)^2 + (yP)]$ and $P = (F_o^2 + 2F_c^2) / 3$; x and y are the respective weight coefficients (see the CIFs).

The intensity data were collected using a Bruker APEX diffractometer, equipped with monochromatized Mo K α radiation, $\lambda = 0.71073$ Å. Processing of raw data and absorption correction were handled with SAINT and SADABS software packages, respectively. Crystal structures were solved by the intrinsic phasing method using SHELXT, and refined by full-matrix least-squares methods on F^2 with SHELXL. Atomic coordinates were standardized, and the atomic labels were set to be consistent with previous studies [25]. Selected details of the data collection and relevant crystallographic parameters [30] for all four samples are given in Table 1.

Electronic Structure Calculations

To calculate the electronic density of states and band structure of disorder-free Ba₂LiGe₃, we used the Stuttgart TB-LMTO-ASA code with the local density approximation. Experimental unit cell parameters and atomic coordinates from sample D were used as the input parameters. In order to satisfy the atomic sphere approximation (ASA), we employed the von Barth-Hedin functional [31], and introduced empty spheres to the calculation. $4 \times 4 \times 4$ k -point grid for the Brillouin zone integrations was used to accurately calculate the Fermi surface. The Fermi level was selected as the energy reference ($E_F = 0$ eV).

Results and Discussion

Notes on the Synthesis and the Literature Data Concerning the Binary Ba–Ge, Li–Ge, and the Ternary Ba–Li–Ge Compounds

As described in the introduction, for a number of years, we have been actively studying the lithiation behavior of Ba–Ge clathrates [27–29]. During the work, we noticed some difficulties with the interpretation of our own experimental results that mostly stem from the fact that the phase space in the Ba–Li–Ge system is not widely explored (thus far). Besides our own recent discovery of the type-I clathrate Ba₈Li₅Ge₄₁ (= Ba₈Li_xGe_{46-x} with $x \approx 5$), only three other ternary phases with different Ba/Li/Ge ratios have been reported, with the first one discovered in 1996. A schematic phase diagram is shown in Figure 1. We caution the reader that one of the compounds on the plot, BaLiGe₂, appears to have only been obtained from an experiment containing Na [26]. Although presumed to be a ternary phase, we have never encountered that compound as a side product in our experiments, while the other two of the above-mentioned Ba–Li–Ge ternaries were often found. Inconsistencies like that provide complications for both the experimentalists and theorists, and need to be clarified in future works.

When undertaking exploratory work in ternary and higher systems, one also needs to be aware of the binaries too. The phase space in the binary Ba–Ge and Li–Ge systems appears to be better mapped compared to the Ba–Li–Ge system. There are several Ba–Ge binary phases which have been reported to date—BaGe [21], BaGe₂ [22], Ba₂Ge [32], Ba₅Ge₃ [33], Ba₆Ge₂₅ [34,35], Ba₈Ge₄₃ [36,37]. In addition, in recent years, BaGe₃ [38], BaGe₅ [39], and BaGe₆ [40] have been reported as phases stabilized by high pressure.

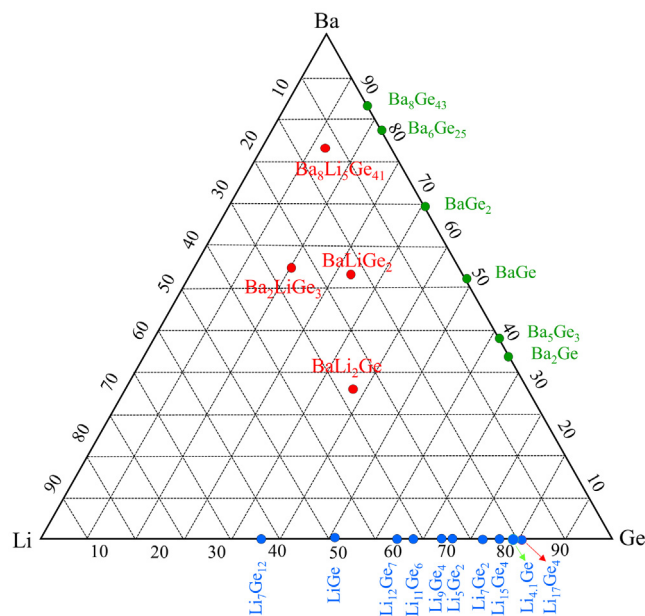


Figure 1. Ba–Li–Ge compositional diagram. The Ba–Ge phases obtained via high-pressure synthesis are not indicated.

The number of indicated Li–Ge binary phases in Figure 1 is greater [17,41–48], but there is a caveat—some of the stated compositions—Li₇Ge₁₂ [43], LiGe [17], Li₅Ge₂ [29], Li₁₂Ge₇ [44], Li₉Ge₄ [45], Li₁₁Ge₆ [46], Li₇Ge₂ [47], Li₁₅Ge₄ [41], Li₁₇Ge₄ [42], Li_{-4.1}Ge [42] are still subject to outright controversies. For instance, older entries in crystallographic databases exist for the cubic phase Li₂₁Ge₅ (also referred to as Li₂₂Ge₅ or Li₂₀Ge₅), which has been reinvestigated in 2001 by Nazar *et al.* and reformulated as Li₋₁₇Ge₄ [48]. In 2016, Fässler *et al.* [42] redid the cubic Li₁₇Ge₄ crystal structure and noted that the earlier reports with partially occupied Li sites could not be replicated. In the same work, another Li-rich phase, the orthorhombic Li_{-4.1}Ge (Li₋₁₇Ge₄), which was previously omitted in the experimental or computationally predicted phase diagrams [49,50], was identified and structurally characterized. Yet, computational work from 2018 indicates a different ground state for Li₄Ge [51], with the possibility for pressure-induced phase transition.

Some less Li-rich phases, such as Li₁₁Ge₆ [46] for example, have never been re-synthesized and experimentally reproduced. We have tried numerous times and from those attempts have identified a phase (with Li : Ge ratio of ca. 1.8 : 1), whose preliminary structure (from single-crystal X-ray diffraction data) is akin, but the identical to the published Li₁₁Ge₆ crystal structure.

Another interesting twist concerning binary lithium germanides involves the rhombohedral Li₅Ge₂ phase, predicted by theory in 2014 [49], and experimentally confirmed by us in 2020 [29]. There is mounting evidence that the “known” crystal structure of Li₅Ge₂ needs another look since the phase might be better described as Li_{5-x}Ge_{2+x}, i.e., there is a small Li/Ge disorder just like the disorder that is at the core of this paper. Based on the still ongoing studies, it is likely that the computationally predicted hexagonal Li₇Ge₃ [49] is actually Li_{5-x}Ge_{2+x} with $x \approx 0.1$. In the same context, it also appears that the structure of Li₇Ge₂ [47] must be revisited as another example for a phase with Li/Ge

disorder. If the disorder and the structure are confirmed, then, $\text{Li}_{7-x}\text{Ge}_{2+x}$ may be suggested to be the experimental validation of the computationally predicted $\text{Li}_{13}\text{Ge}_4$ phase [49].

On this note, we will recall that Li atoms replacing Ge atoms in a crystal structure of a solid is a rare phenomenon, but not without precedents. For instance, recently, when we reported on $\text{Ba}_8\text{Li}_5\text{Ge}_{41}$ (actual chemical formula $\text{Ba}_8\text{Li}_x\text{Ge}_{46-x}$ ($x < 5.33$) with the type-I clathrate structure [27], based on single-crystal X-ray diffraction work, we concluded that one of the crystallographic sites nominally taken by Ge (6c) shows co-occupation by lithium atoms that are sharing the chemistry with germanium atoms. While unusual, another example of this kind of Li/Ge disorder has been seen in the similar type-I clathrate $\text{K}_8\text{Li}_x\text{Ge}_{44-x/4}\square_{2-3x/4}$

($0 < x < 2.67$; \square denotes a vacancy) [52,53]. In the latter case, the gradual incorporation of Li atoms into the 6c site has suggested that the Li atoms first fill the vacancies on that particular site [52], before more Ge atoms are substituted by Li. We posit that such crystal chemistry is more widespread than originally thought, and with this paper, we will demonstrate that the stipulated Li/Ge disorder in $\text{Ba}_2\text{Li}_{1-x}\text{Ge}_{3+x}$ is discernable based on careful refinements of the crystal structure from single-crystal X-ray diffraction data. Even without the refinements, the tell-tale signs of Li/Ge disorder are the subtle peak-shifts in the powder X-ray diffraction patterns, offering small clues that changes in the unit cell volume of $\text{Ba}_2\text{Li}_{1-x}\text{Ge}_{3+x}$ occur when the experimental conditions are slightly varied.

Table 2. Atomic coordinates and equivalent isotropic displacement parameter for $\text{Ba}_2\text{Li}_{1-x}\text{Ge}_{3+x}$. The synthesized samples are labeled as A, B, C, and D. Li atoms in all cases are refined isotropically ($U_{\text{eq}} = U_{\text{iso}}$) and for them, the value is constrained to the average U_{eq} value for the heavy atoms in the structure.

Sample A						
Atom	Wyckoff Site	x	y	z	$U_{\text{eq}}/\text{\AA}^2$	
Ba1	16g	1/8	1/8	0.99954(3)	0.0147(2)	
Ba2	16g	1/8	1/8	0.50082(3)	0.0175(2)	
Li ^[a]	16f	1/8	0.4591(7)	1/8	0.015	
Ge1	16f	1/8	0.28719(7)	1/8	0.0152(3)	
Ge2	32h	0.3681(1)	0.04389(5)	0.12117(5)	0.0157(3)	
Sample B						
Ba1	16g	1/8	1/8	0.00025(3)	0.0130(2)	
Ba2	16g	1/8	1/8	0.50083(3)	0.0149(2)	
Li ^[a]	16f	1/8	0.4589(7)	1/8	0.013	
Ge1	16f	1/8	0.28760(7)	1/8	0.0130(3)	
Ge2	32h	0.36859(9)	0.04395(5)	0.12118(4)	0.0137(2)	
Sample C						
Ba1	16g	1/8	1/8	0.00154(3)	0.0118(2)	
Ba2	16g	1/8	1/8	0.50073(3)	0.0121(2)	
Li ^[a]	16f	1/8	0.4574(7)	1/8	0.012	
Ge1	16f	1/8	0.28797(7)	1/8	0.0121(2)	
Ge2	32h	0.36939(9)	0.04363(5)	0.12105(4)	0.0124(2)	
Sample D						
Ba1	16g	1/8	1/8	0.00129(3)	0.0123(2)	
Ba2	16g	1/8	1/8	0.50078(3)	0.0130(2)	
Li ^[a]	16f	1/8	0.4572(10)	1/8	0.012	
Ge1	16f	1/8	0.28782(7)	1/8	0.0126(2)	
Ge2	32h	0.36885(9)	0.04377(5)	0.12091(4)	0.0129(2)	

^[a] Refined occupancies are as follows: sample A, Li : Ge = 0.953(4) : 0.047; sample B, Li : Ge = 0.964(4) : 0.036; sample C, Li : Ge = 0.964(3) : 0.036; and for sample D, Li is 100%.

Crystal Structure

Crystal structures of all four synthesized samples were analyzed based on single-crystal XRD data. Powder X-ray diffraction patterns of our synthesized samples are presented in figure S1 (Supplementary information) and show the phase purity in bulk.

Before we begin with the discussion on the Li/Ge disorder in $\text{Ba}_2\text{Li}_{1-x}\text{Ge}_{3+x}$, let us first briefly recap the idealized crystal structure of Ba_2LiGe_3 , as reported in 1996 [25]. The phase crystallizes in the orthorhombic space group $Fddd$ (no. 70). There are five independent sites in the asymmetric unit (Table 2); including two barium atoms (at sites 16g), two germanium atoms (one at site 16f and another at site 32h) and one lithium atom (at site 16f). The most interesting structural features, as noted in the earlier publication, are the planar $[\text{Ge}_6]^{10-}$ anions (Figure 2). In some way, they are akin to the C_6H_6 molecule, i.e., the Ge–Ge bonding has some aromatic character to it and both follow the Hückel $4n+2$ rule for aromatic systems. The difference is that benzene has 6 electrons in conjugation ($n = 1$), while $[\text{Ge}_6]^{10-}$ has 10, i.e., $n = 2$. The π -aromaticity of the $[\text{Ge}_6]^{10-}$ anions has also been studied by the group of R. Nesper on the examples of $\beta\text{-Sr}_2\text{LiGe}_3$ and $\gamma\text{-Sr}_2\text{LiGe}_3$ [54]. The subject of inorganic aromaticity has been reviewed by Boldyrev *et al* [55] and appears that a number of Zintl phases feature planar conjugated moieties that have aromatic organic analogs. For example, the pentagonal $[\text{Sn}_5]^{6-}$ and $[\text{Pb}_5]^{6-}$ can be considered to be inorganic analogues of cyclopentadienyl anion $[\text{C}_5\text{H}_5]^-$ [12,56]. Similar traits with bonding that can be elaborated in terms of the Hückel rule exist in $\beta\text{-K}_4\text{P}_6$ [57], where $[\text{P}_6]^{4-}$ rings exist and can be viewed as isostructural and isoelectronic with the $[\text{Ge}_6]^{10-}$ anions.

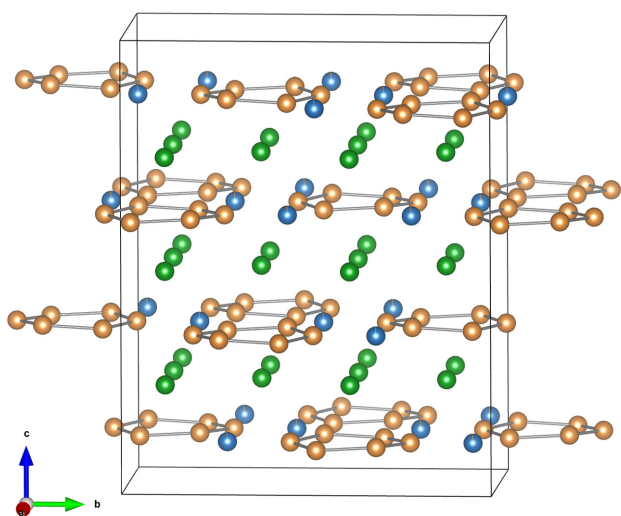


Figure 2. Schematic representation of the orthorhombic crystal structure of Ba_2LiGe_3 (space group $Fddd$). Green, blue and golden colors represent Ba, Li and Ge atoms, respectively.

Since the Ge atoms are nearly in the same plane with the Li atoms, the 6-member Ge-rings can also be viewed as interconnected by the Li-atoms, resulting in graphite-like nets; this description assumes that both types of atoms are covalently bonded and Li is not just a cation. The 2D-nets then must be considered as $[\text{LiGe}_3]^{4-}$ and they have a honeycomb-like topology (Figure 3). The Li/Ge layers are stacked along the c -direction and are separated by slabs of Ba^{2+} cations. This arrangement bears some analogy with the structure of the quaternary phase $\text{BaMg}_2\text{Li}_2\text{Ge}_2$, where Ba atoms are situated in between almost flat $[\text{Li}_2\text{Ge}_2]$ layers having a 3-fold symmetry; by comparison, the structures of the isotypic $\text{BaLi}_2\text{Cd}_2\text{Ge}_2$ and $\text{BaLi}_2\text{In}_2\text{Ge}_2$ show puckered $[\text{Cd}_2\text{Ge}_2]$ and $[\text{In}_2\text{Ge}_2]$ layers [58,59]. Thus, the structure can be described as $(\text{Ba}^{2+})_2(\text{LiGe}_3)^{4-}$, i.e., Ba_2LiGe_3 is a typical Zintl phase.

However, as noted in the introduction, there exists a significant difference in the lattice parameters between the reported ones ($a = 8.901(1) \text{ \AA}$, $b = 15.469(2) \text{ \AA}$, and $c = 19.4300(20) \text{ \AA}$) and what is listed in Table 1. Notwithstanding the temperature difference, some of the variations in the unit cell are so big that they can be easily spotted by just a visual inspection of the PXRD patterns (Figure S1b). For instance, one can see the shift of the highest intensity peak (the zoomed-in region from 29 to 31° in 2θ); these are clearly related to the change in unit cell volume in response to the change in the synthetic conditions. This is where the question about the potential for Li/Ge disorder in $\text{Ba}_2\text{Li}_{1-x}\text{Ge}_{3+x}$ arises naturally.

Refining Li occupancies by X-ray crystallography alone is not a reliable method for ascertaining the structure when Li-disorder is suspected. This required us to carry out experiments with the slightly Li-deficient $\text{Ba}_2\text{Li}_{1-x}\text{Ge}_{3+x}$ ($x < 0.1$) and the slightly Li-rich $\text{Ba}_2\text{Li}_{1+x}\text{Ge}_{3-x}$ ($x < 0.1$) nominal compositions and to carefully compare the structure refinement results in that context. Doing so indicated that excess Li in the nominal composition has little-to-no-effect on the refined structure (N.B. von Schnering's communication indicates that their sample was also prepared from a nominal mixture with 5% excess lithium to "avoid Li loss at high temperature" [25]). By comparison, the crystals from reactions with slightly less than the ideal stoichiometric amount of Li show subtle differences in the structure refinements that manifest themselves in residual electron density on the Li site (*vide infra*), in addition to the already noted volume changes. Taking the above into an account suggests that one (or both) of the Ge sites being partially by Li atoms is an improbable proposition. The hypothesis that the "heavy" Li atom site is originated from it being partially occupied by Ge atoms is considered more likely, therefore, the formula $\text{Ba}_2\text{Li}_{1-x}\text{Ge}_{3+x}$ is deemed most appropriate. In the next paragraphs, we focus the attention on how we interpreted the data that helped establish the model and allowed us to resolve the disorder.

First and most important observation—refinement of occupation factors for either Ba or Ge atoms proved no statistically significant deviations from 100% for *any* of the four data sets (Table 1 and 2). For the lithium atoms, however, in three of the four cases, refinements of the occupation factors

resulted in unphysical (more than 100%) values of 110–160%. This outcome indicated the possibility that heavier atoms partially occupy the 16f site assigned to the light Li atom.

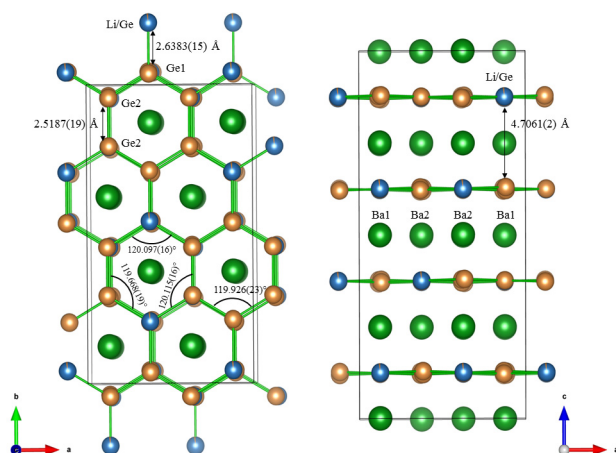


Figure 3. Crystal structure of $\text{Ba}_2\text{Li}_{1-x}\text{Ge}_{3+x}$ projected down the c - and b -directions. Selected distances and angles are denoted. Green, blue and golden colors represent Ba, Li and Ge atoms, respectively.

Considering the distances to nearest neighbors, on the order of 2.6 Å, the large Ba taking that position can be ruled out, leaving Ge as the only possibility (Nb from the container can be dismissed, since unphysical Li occupation factor of the same magnitude was observed for a sample prepared in carbon-coated silica tube). Indeed, introducing statistical admixture of Li and Ge at site 16f contributed to a much better refinement results, with R -values improving for three of the four samples.

The disorder Li/Ge is not as pronounced as in $\text{Ba}_8\text{Li}_x\text{Ge}_{46-x}$, where Li/Ge ratio on site 6c was ca. 80:20%; in $\text{Ba}_2\text{Li}_{1-x}\text{Ge}_{3+x}$ the highest substitution level was found to be about ca. 5%. The reader must be cautioned that the refined level of Li/Ge admixing could be significantly different if one considers the possibility that there are defects on the Li site, in addition to the substitutional disorder. This conjecture can be made following the case of type-I clathrate $\text{K}_8\text{Li}_x\text{Ge}_{44-x/4}\square_{2-3x/4}$ ($0 < x < 2.67$; \square denotes a vacancy) [52,53], and if so, the actual formula would be $\text{Ba}_2\text{Li}_{1-x}\square_y\text{Ge}_{3+x}$ or $\text{Ba}_2\text{Li}_{1-x}\text{Ge}_{3+y}$, where x and y are independent variables ($x > y$ will describe the situation with vacancies present on the Li site, but will still account for the “heavy” Li encountered during the refinements). However it is difficult to conclude the presence of vacancies with the data available at present.

As we noticed a gradual change in lattice parameters from samples A to D (Table 1) (a - and b - cell parameters are decreasing and c - cell parameter is increasing), we tried to correlate the $\text{Ba}_2\text{Li}_{1-x}\text{Ge}_{3+x}$ ($x < 0.05$) model to this systematic change. The refinement results for A, B, and C samples show approximately the same refined compositions; however, considering that the size of the Li is slightly larger than that of Ge [60], it appears that the smallest volume (sample A) ought to have the smallest amount Li. These findings are also in an agreement with the fact that the A and B samples were the slightly Li-deficient ones, based on the loaded compositions. For sample D, the largest cell volume and no significant deviation of the Li occupancy from 100% indicate that the composition is very close to the ideal stoichiometric.

Table 3. Selected interatomic distances (Å) in $\text{Ba}_2\text{Li}_{1-x}\text{Ge}_{3+x}$.

Atom 1	Atom 2	Sample A	Sample B	Sample C	Sample D	Sample from ref.25
Ba1–	Ge1 (x2)	3.4744(15)	3.4737(17)	3.4688(8)	3.4673(10)	3.4756(9)
	Ge1 (x2)	3.5334(11)	3.5441(13)	3.5642(7)	3.5664(7)	3.5811(6)
	Ge2 (x2)	3.5159(15)	3.5168(17)	3.5169(8)	3.5159(10)	3.4143(10)
	Ge2 (x2)	3.4174(15)	3.4148(16)	3.4093(8)	3.4081(10)	3.5243(10)
	Li (x4)	3.5010(5)	3.5163(5)	3.5422(2)	3.5379(3)	3.5378(16)
Ba2–	Ge1 (x2)	3.5499(11)	3.5515(13)	3.5560(7)	3.5560(7)	3.5699(6)
	Ge2 (x2)	3.4833(15)	3.4820(17)	3.4842(8)	3.4832(10)	3.4998(10)
	Ge2 (x2)	3.5086(16)	3.5095(17)	3.5087(9)	3.5088(10)	3.5001(10)
	Ge2 (x2)	3.5788(15)	3.5819(17)	3.5902(8)	3.5893(10)	3.5810(1)
	Li (x4)	3.5178(5)	3.5210(11)	3.5200(4)	3.5272(3)	3.5266(14)
Ge1–	Ge2 (x2)	2.5048(16)	2.5080(17)	2.5069(7)	2.5066(10)	2.5067(10)
	Li	2.6383(15)	2.6310(15)	2.6242(6)	2.6056(10)	2.5860(5)

Ge2–	Ge2	2.5048(16)	2.5080(17)	2.5069(7)	2.5066(10)	2.5067(10)
	Ge2	2.5187(19)	2.5150(2)	2.5136(9)	2.5130(12)	2.5203(11)
	Li	2.6578(8)	2.6452(8)	2.6261(3)	2.6330(3)	2.6676(24)
Layer-to-layer		4.7061(2)	4.7271(4)	4.7600(2)	4.7626(3)	4.7781(5)

How do these occupational disorder changes affect the rest of the structure? Recall that the six-member rings of germanium atoms, interconnected by lithium atoms, make layers in the *ab*-plane (with stacking occurring along the *c*-direction). The barium atoms are positioned in between the [LiGe₃] layers (Figure 3). They can be described as forming an array of fused trigonal prisms with base-edges of ca. 4.5 Å and approximately 4.7–4.8 Å in height. Each Ba₆ prism is centered by Ge or Li atom, a prototypical AIB₂ type arrangement. Within the Ge cyclic system, the $d_{\text{Ge1-Ge2}}$ and $d_{\text{Ge2-Ge2}}$ fall in the narrow range of ca. 2.50–2.52 Å, respectively (Table 3). The values match well those reported earlier [25]. Ge–Ge distances are also comparable to the ones in many binary germanides [18,33–43]. This marginal range of Ge–Ge bond lengths can be also compared to that of the isotopic γ -Sr₂LiGe₃ [54].

A slight but systematic decrease of $d_{\text{Ge2-Ge2}}$ is noticeable, as its value is equal to ca. 1/6 of the *b*-axis parameter. The Li–Ge1 bonds are also parallel to the *b*-axis (Figure 3), therefore $d_{\text{Li-Ge1}}$ were found to be decreasing from A to C samples (Table 3). Bond angles of the planar [Ge₆]¹⁰⁻ anions are very close to 120° (Figure 3), supporting the notion for sp²-hybridization, expected for an aromatic system. Including the Li-atoms in the covalent bonding allows for an extension of the conjugation within the entire honeycomb-like [LiGe₃]⁴⁻ layer, as evident from the <Ge1-Ge2-Li and <Ge2-Li-Ge1 angles which are also very close to 120° (Figure 3a). Nevertheless, the rings with Li and Ge atoms are nearly flat with a torsion angle of ca. ±0.09°, the rings made from Ge atoms only are slightly puckered with a torsion angle of ±3.9–4.0°, close to the reported value reported by von Schnering's team [25]. On the other hand, layer-to-layer separation in *c*-direction is increasing systematically (Table 3). Layer-to-layer distance shows a relationship with the *c*-axis parameter in almost a linear fashion. This scaling is in correlation with the $d_{\text{Ba-Ge}}$ and $d_{\text{Ba-Li}}$, refined to be in the ranges 3.47–3.56 Å and 3.50–3.55 Å (Table 3).

Before we begin with the discussion on the electronic structure, let us briefly recap the counting of the valence electrons that was mentioned earlier. If the electron count is approached from the viewpoint of isolated [Ge₆]¹⁰⁻ anions where the Ge–Ge bonding has some aromatic character, then the formula Ba₂LiGe₃ can be rationalized as (Ba²⁺)₄(Li⁺)₂[Ge₆]¹⁰⁻. Notice that this breakdown cannot happen if one treats all Ge–Ge bonds as two-center-two-electron interactions—in this case, the partitioning scheme following the Zintl concept [15,16] must be (Ba²⁺)₄(Li⁺)₂(2*b*-Ge²⁻)₆, where the symbol 2*b* denotes a Ge atom with 2 bonds (and two lone pairs). This clearly suggests

electron deficiency and such compound is unlikely to be stable. On the other hand, if the Ge–Ge bonding is considered as intermediate between the two extremes, then, the drive of the Ba₂Li_{1-x}Ge_{3+x} structure to rid itself of some Li atoms in favor of adding some Ge atoms in their place can be easily understood—this change in valence electrons can lead to a structure with an overall greater electronic stability. We can even consider the hypothetical Ba₂Li_{1-x}Ge_{3+x} end member with *x* = 1, which will have the chemical formula Ba₂Ge₄ (= BaGe₂). Such compound will feature a structure with 2D-nets [Ge₂]²⁻ (graphene-like) and will be analogous to a large number of germanides forming with the AIB₂ structure (recall that the array of fused Ba₆ prisms, centered by Ge or Li atoms, suggests that the structure of Ba₂Li_{1-x}Ge_{3+x} can also be viewed as an ordered, orthorhombically distorted variant of the AIB₂ structure). One would not expect BaGe₂ to be isotopic with AIB₂, since AGe₂ (A = alkaline-earth metal) form puckered 2D-nets [Ge₂]²⁻, but the application of pressure can induce “flattening” of the layers, as demonstrated not too long ago for BaSi₂ and BaGe₂ [61].

Electronic Structure

In this section we provide some insights on the electronic band structure and bonding nature of this phase. Therefore, we performed a computational analysis using density functional theory, as implemented in the LMTO method. As stated, the computational work did not include modeling of the Li/Ge disorder, and we only considered the disorder-free Ba₂LiGe₃ structure. The results are graphically summarized in Figure 4 and Figure 5, where emergence of a bandgap is hardly distinguishable—we can call this dip in the DOS at the Fermi level a pseudogap [62,63].

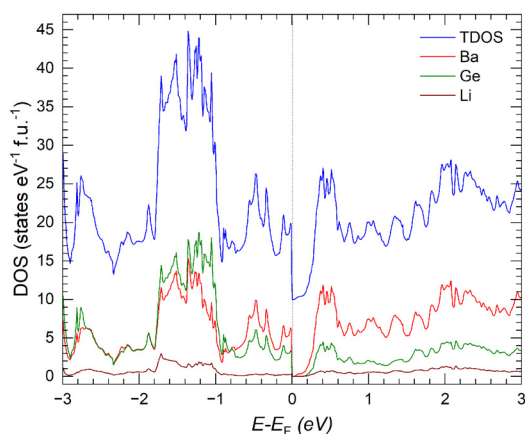


Figure 4. The stacked atom-projected electronic density of states (DOS) for disorder-free Ba_2LiGe_3 .

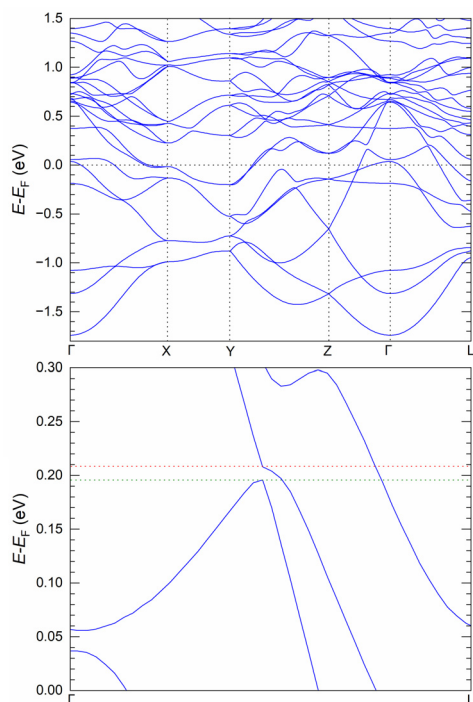


Figure 5. Electronic band structure of disorder-free Ba_2LiGe_3 and (b) plotted gap between Γ and L for the same phase.

The majority of the states near the bottom of the conduction band are contributed by Ba orbitals, with minor contribution from Ge. The states close to the valence band maximum are contributed mainly by Ge orbitals, some Ba contributions must also be noted. The Li atoms have very minor contributions near the Fermi level. The major overlap of Ba and Ge evidenced in the valence band (states between -3 eV and 0 eV; recall that we plot $E-E_F$ and zero is the Fermi level) suggests that there are some covalent features of the interactions between Ba and Ge atoms.

Figure 5 shows the electronic band structure of disorder-free Ba_2LiGe_3 in momentum space. As evident from the plot, the valence and the conduction bands are crossing the Fermi level, but a slightly distinguishable gap between two bands can be noticed between Γ and L. From the figure, one can see that the gap between the valence (green dotted line) and the conduction bands (red dotted line) is only about 0.01 eV. Therefore, the disorder-free Ba_2LiGe_3 is predicted to be semi-metallic. However, von Schnering's original article claimed Ba_2LiGe_3 to be a narrow band semiconductor ($E_g \approx 80$ meV) [25], although details of the calculations were not presented and it is unclear how this bandgap was identified. It is noteworthy that metallic behavior is also shown in the Sr_2LiGe_3 analogue [54]. For the latter, it has been shown that the DOS around the Fermi level is mainly contributed by germanium atoms with small admixing by strontium (without any gap). In the present case, the states around the Fermi level are contributed from both Ge-p and Ba-d states (Figure S2). A close inspection of the partial DOS curves indicates the existence of a small gap for the Ge states, but no gap for the barium states, which is what likely leads to the overall pseudogap. The impact of the Li/Ge admixing on the electronic structure is unknown at present—given the very small amount of Ge on the Li site, calculations with the LMTO code would require the tedious (and likely erroneous) construction of complex ordered superstructures, which we did not attempt to do. We can speculate that the Li/Ge disorder would lead to an energetically favored situation, like e.g. settling of E_F within a deep local minimum or perhaps even opening of a small band gap. Further computational work on $\text{Ba}_2\text{Li}_{1-x}\text{Ge}_{3+x}$ is called for.

To further interrogate the subtle covalent features of Ba–Ge bonding, we next consider their crystal orbital Hamiltonian population curves (COHP) [64], plotted in Figure 6. All the atomic interactions are nearly optimized at the Fermi level, except for the Ge–Ge interactions. No antibonding states for Ba–Ge, Ba–Li and Li–Ge interactions can be observed below the Fermi level. All four types of interactions show some bonding character above the Fermi level.

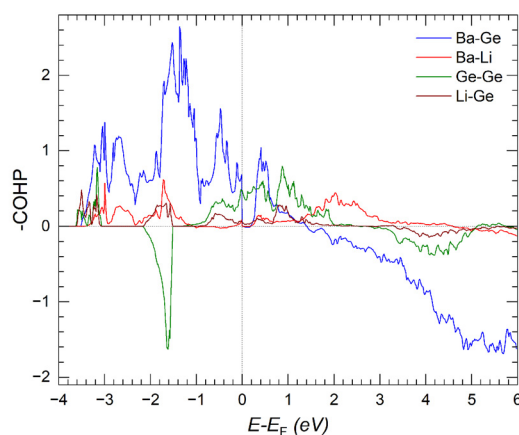


Figure 6. Crystal orbital Hamiltonian population curves for Ba–Ge, Ba–Li, Ge–Ge and Li–Ge interactions in disorder-free Ba_2LiGe_3 .

Conclusion

The structure of the Ba_2LiGe_3 that has been known for almost 30 years was shown to be a subject of small Li/Ge disorder. We synthesized four different samples with slightly Li-deficient $\text{Ba}_2\text{Li}_{1-x}\text{Ge}_{3+x}$ and Li-rich $\text{Ba}_2\text{Li}_{1+x}\text{Ge}_{3-x}$ ($x < 0.1$) nominal compositions. All obtained crystals were characterized by single-crystal and powder X-ray diffraction. The results do confirm a small homogeneity range for $\text{Ba}_2\text{Li}_{1-x}\text{Ge}_{3+x}$ ($x < 0.05$), which is clearly demonstrated in the variations of the unit cell volumes. There are concomitant changes for the refined lengths of the Li–Ge and Ge–Ge bonds too, specifically, the change of *a*- and *b*-unit cell parameter can be established in terms of the alteration of Ge–Ge and Li–Ge bond lengths; the *c*-parameter is in correlation with the layer to layer distances. In the honeycomb-like layers, the $[\text{Li}_2\text{Ge}_4]$ six-member rings appear to be nearly flat, while the presumed aromatic $[\text{Ge}_6]^{10-}$ cyclic anions are slightly puckered. The chemical formula of the idealized Ba_2LiGe_3 composition can be partitioned following the Zintl concept as $(\text{Ba}^{2+})_4(\text{Li}^+)_2[\text{Ge}_6]^{10-}$, taking into an account the Hückel rules for aromatic systems $4n+2$ for $n = 2$.

The presently uncovered and crystallographically studied case of Li metal atoms and Ge atoms sharing chemistry in the solid state adds a layer of additional complexity as it slightly alters the above description. The $\text{Ba}_2\text{Li}_{1-x}\text{Ge}_{3+x}$ phase is an intermediate between the idealized Ba_2LiGe_3 ($x = 0$) and Ba_2Ge_4 ($x = 1$) compositions with $[\text{Ge}_6]^{10-}$ isolated anions and $[\text{Ge}_2]^{2-}$ sheets.

Supporting Information

Powder XRD data for several $\text{Ba}_2\text{Li}_{1-x}\text{Ge}_{3+x}$ compositions (Figure S1) and electronic density of states (DOS) for idealized, disorder-free Ba_2LiGe_3 focusing on the Ge 4s, 4p and Ba 5d contributions (Figure S2).

Acknowledgements

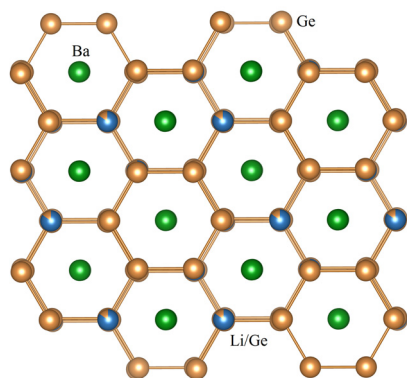
This work was supported by the US National Science Foundation (NSF) through grant DMR-2004579. The authors thank Amanda Childs for early exploratory work in the Ba–Li–Ge system.

Keywords: crystal structure • germanium • lithium • Zintl phases

- [1] J. D. Corbett, *Angew. Chem. Int. Ed.* **2000**, *39*, 670, and references therein.
- [2] J. D. Corbett, *Inorg. Chem.* **2010**, *49*, 13, and references therein.
- [3] O. Janka, S. M. Kauzlarich, *Zintl Compounds, Encyclopedia of Inorganic and Bioinorganic Chemistry*, Wiley, Hoboken, NJ, **2014**, pp. 1–14, and references therein.
- [4] H. Schäfer, B. Eisenmann, W. Müller, *Angew. Chem. Int. Ed. Engl.* **1973**, *12*, 694–712, and references therein.
- [5] A. M. Guloy, *Polar Intermetallics and Zintl Phases along the Zintl Border*. in *Inorganic Chemistry in Focus III* (Eds.: G. Meyer, D. Naumann, L. Wesemann), Wiley-VCH Verlag GmbH & Co: Weinheim, Germany, **2006**, pp. 157–171, and references therein.
- [6] R. Nesper, *Angew. Chem. Int. Ed. Engl.* **1991**, *30*, 789–817, and references therein.
- [7] S. Bobev, S. C. Sevov, *J. Am. Chem. Soc.* **2002**, *124*, 3359.
- [8] L. M. Scherf, A. J. Karttunen, O. Pecher, P. C. M. M. Magusin, C. P. Grey, T. F. Fässler, *Angew. Chem. Int. Ed.* **2016**, *55*, 1075.
- [9] S. Bobev, S. C. Sevov, *Angew. Chem. Int. Ed.* **2001**, *40*, 1507.
- [10] L. M. Scherf, M. Zeilinger, T. F. Fässler, *Inorg. Chem.* **2014**, *53*, 2096.
- [11] R. Nesper, A. Currao, S. Wengert, *Eur. J. Inorg. Chem.* **1998**, *4*, 2251.
- [12] I. Todorov, S. C. Sevov, *Inorg. Chem.* **2004**, *43*, 6490.
- [13] A. Ovchinnikov, S. Bobev, *Dalton Trans.* **2019**, *48*, 14398.
- [14] M.-H. Ge, J. D. Corbett, *Inorg. Chem.* **2007**, *46*, 4138.
- [15] S. M. Kauzlarich, *Chemistry, Structure and Bonding of Zintl Phases and Ions*, VCH, New York, **1998**.
- [16] R. Nesper, *Z. Anorg. Allg. Chem.* **2014**, *640*, 2639.
- [17] J. Evers, G. Oehlinger, G. Sextl, H. O. Becker, *Angew. Chem.* **1987**, *99*, 69.
- [18] a) N. D. Cultrara, Y. Wang, M. Q. Arguilla, M. R. Scudder, S. Jiang, W. Windl, S. Bobev, J. E. Goldberger, *Chem. Mater.* **2018**, *30*, 1335; b) P. H. Tobash, S. Bobev, *J. Solid State Chem.* **2007**, *180*, 1575.
- [19] A. Betz, H. Schäfer, A. Weiss, *Z. Naturforsch. B.* **1967**, *22*, 103.
- [20] a) F. Merlo, M.L. Fornasini, *J. Less-Common Met.* **1986**, *119*, 45; b) N.-T. Suen, S. Bobev, *Chem.* **2022**, *4*, 1429.
- [21] W. Rieger, E. Parthé, *Acta. Cryst.* **1967**, *22*, 919.
- [22] A. Betz, H. Schäfer, A. Weiss, R. Wulf, *Z. Naturforsch. B.* **1968**, *23*, 878.
- [23] V. Queneau, S. C. Sevov, *Angew. Chemie. Int. Ed.* **1997**, *36*, 1754.
- [24] D. Stoiber, M. Bobnar, P. Höhn, R. Niewa, *Z. Naturforsch. B.* **2017**, *72*, 847.
- [25] H.-G. von Schnering, U. Bolle, J. Curda, K. Peters, W. Carrillo-Cabrera, M. Somer, M. Schultheiss, U. Wedig, *Angew. Chem. Int. Ed. Engl.* **1996**, *35*, 984.
- [26] D.-G. Park, Y. Dong, F. J. DiSalvo, *J. Alloys Compd.* **2009**, *470*, 90.
- [27] K. Ghosh, A. Ovchinnikov, M. Baitinger, M. Krnel, U. Burkhardt, Y. Grin, S. Bobev, *Dalton Trans.* **2023**, *52*, 10310.
- [28] A. Dopiika, R. Zhao, J. M. Weller, S. Bobev, X. Peng, C. K. Chan, *ACS Appl. Mater. Inter.* **2018**, *10*, 37981.
- [29] A. Dopiika, A. B. Childs, S. Bobev, C. K. Chan, *Chem. Mater.* **2020**, *32*, 9444.
- [30] Deposition numbers 2284140 (for **A**), 2284141 (for **B**), 2284142 (for **C**), and 2284143 (for **D**) contain the supplementary crystallographic data for this paper. These data are provided free of charge by the joint Cambridge Crystallographic Data Centre and Fachinformationszentrum Karlsruhe [Access Structures](#) service.
- [31] U. Von Barth, L. Hedin, *J. Phys. C: Solid State Phys.* **1972**, *5*, 1629.
- [32] K. Turban, H. Schäfer, *Z. Naturforsch. B* **1973**, *28*, 220.
- [33] R. Nesper, F. Zürcher, *Z. Krist.* **1999**, *214*, 22.
- [34] S.-J. Kim, S. Hu, C. Uher, T. Hogan, B. Huang, J. D. Corbett, M. G. Kanatzidis, *J. Solid State Chem.* **2000**, *153*, 321.
- [35] W. Carrillo-Cabrera, J. Curda, H.-G. von Schnering, S. Paschen, Y. Grin, *Z. Krist.* **2000**, *215*, 207.
- [36] W. Carrillo-Cabrera, S. Budnyk, Y. Prots, Y. Grin, *Z. Anorg. Allg. Chem.* **2004**, *630*, 2267.
- [37] W. Carrillo-Cabrera, J. Curda, K. Peters, S. Paschen, M. Baenitz, Y. Grin, H.-G. von Schnering, *Z. Krist.* **2000**, *215*, 321.

- [38] H. Fukuoka, Y. Tomomitsu, K. Inumaru, *Inorg. Chem.* **2011**, *50*, 6372.
- [39] R. Castillo, W. Carrillo-Cabrera, U. Schwarz, Y. Grin, *Inorg. Chem.* **2015**, *54*, 1019.
- [40] L. Akselrud, A. Wosylus, R. Castillo, U. Aydemir, Y. Prots, W. Schnelle, Y. Grin, U. Schwarz, *Inorg. Chem.* **2014**, *53*, 12699.
- [41] a) Q. Johnson, G. S. Smith, D. Wood, *Acta Crystallogr.* **1965**, *18*, 131;
b) H. H. Osman, S. Bobev, *Eur. J. Inorg. Chem.* **2022**, *4*, e202100901.
- [42] M. Zeilinger, T. F. Fässler, *Dalton Trans.* **2014**, *43*, 14959.
- [43] F. Kiefer, T. F. Fässler, *Sol. Stat. Sci.* **2011**, *13*, 636.
- [44] L. M. Scherf, N. Riphaus, T. F. Fässler, *Z. Anorg. Allg. Chem.* **2016**, *642*, 1143.
- [45] V. Hopf, H. Schäfer, A. Weiss, *Z. Naturforsch. B* **1970**, *25*, 653.
- [46] U. Frank, W. Müller, *Z. Naturforsch. B* **1975**, *30*, 313.
- [47] V. Hopf, W. Müller, H. Schäfer, *Z. Naturforsch. B* **1972**, *27*, 1157.
- [48] G. R. Goward, N. J. Taylor, D. C. S. Souza, L. F. Nazar, *J. Alloys Compd.* **2001**, *329*, 82.
- [49] A. Morris, C. P. Grey, C. J. Pickard, *Phys. Rev. B* **2014**, *90*, 054111.
- [50] S. Wang, Y. Du, Y. Peng, P. Zhou, X. Yuan, S. Liu, *J. Phase Equilib. Diffus.* **2018**, *39*, 315.
- [51] C. M. Hao, Y. Li, Q. Zhu, X.Y. Chen, Z. X. Wang, Y. L. Li, *Cryst. Eng. Comm.* **2018**, *20*, 5949.
- [52] Y. Liang, B. Böhme, A. Ormeci, H. Borrmann, O. Pecher, F. Haarmann, W. Schnelle, M. Baitinger, Y. Grin, *Chem. Eur. J.* **2012**, *18*, 9818.
- [53] Y. Liang, W. Carrillo-Cabrera, A. Ormeci, B. Böhme, M. Baitinger, Y. Grin, *Z. Anorg. Allg. Chem.* **2015**, *641*, 339.
- [54] Q. Xie, E. C. Reyes, M. Wörle, R. Nesper, *Z. Anorg. Allg. Chem.* **2011**, *637*, 846.
- [55] T. R. Galeev, A. I. Boldyrev, *Comprehensive Inorganic Chemistry II*, **2013**, *9*, 245-275.
- [56] I. Todorov, S. C. Sevov, *Inorg. Chem.* **2005**, *44*, 5361.
- [57] H.-P. Abicht, W. Hönle, H.-G. von Schnering, *Z. Krist.* **1984**, *519*, 7.
- [58] S. Baranets, A. Ovchinnikov, S. Bobev, *Z. Naturforsch. B* **2021**, *76*, 689.
- [59] A. Ovchinnikov, S. Bobev, *Inorg. Chem.* **2019**, *58*, 7895.
- [60] L. Pauling, *The Nature of the Chemical Bonding*, 3rd ed., Cornell Univ. Press Ithaca, NY, USA. 1960, p. 403.
- [61] J. T. Wang, C. Chen, Y. Kawazoe, *Phys. Rev. B.* **2015**, *91*, 054107.
- [62] N. F. Mott, *Rev. Modern Phys.* **1968**, *40*, 677.
- [63] T. Timusk, B. Statt, *Rep. Prog. Phys.* **1999**, *62*, 61.
- [64] S. Steinberg, R. Dronskowski, *Crystals* **2018**, *8*, 225.

Entry for the Table of Contents



The structure of Ba₂Li_{1-x}Ge_{3+x}, emphasizing the honeycomb-like [Li_{1-x}Ge_{3+x}] layers with Li and Ge atoms (denoted in blue and gold) in a partially disordered state.